On the Chromatic Attributes of Early Invasive Skin Melanoma

Gladimir V. G. Baranoski
School of Computer Science, University of Waterloo
Waterloo, Ontario, Canada
gvgbaran@uwaterloo.ca

Petri M. Varsa
School of Computer Science, University of Waterloo
Waterloo, Ontario, Canada
pmvarsa@uwaterloo.ca

***Abstract*—The timely detection of skin melanomas is crucial for their effective treatment and positive prognosis. These lesions are often associated with a dark color, close to pure black, linked to their high melanin content. However, in their early stages, melanoma tumours may be characterized by lighter colors. Despite the medical implications of their appearance, the biophysical factors eliciting their distinct coloration remain to be systematically unveiled. This knowledge gap is significantly tied to the practical difficulties of conducting controlled *in vivo* experiments involving these lesions. In this paper, we aim to further the current understanding about the color variations of early invasive skin melanomas (EISMs). To achieve this objective, we employ an *in silico* investigation approach supported by prior work in this area. More specifically, we examine the impact that physiological and morphological tissue alterations in the EISM lesions, notably involving their dermal blood content, the radius of their scattering-inducing fibrils and the eumelanin to pheomelanin ratios of their pigment-containing organelles, may have on their chromatic attributes. Furthermore, our investigation brings forward practical aspects related to the use of these attributes in the noninvasive screening and predictive analysis of these life-threatening lesions, particularly before the onset of metastasis.**

***Index Terms*—skin melanoma, color, angiogenesis, fibril-induced scattering, *in silico* experiments, predictive simulations.**

I. Introduction

Melanoma is the deadliest type of skin cancer, notably due to its relatively high probability of metastasis, with pathogenic agents spreading to other organs and tissues [1], [2]. Accordingly, its early detection is of vital importance and a number of protocols have been devised for this purpose. The color variations observed in these lesions are among the main signs examined by these protocols [3], [4].

Human skin is generally described, from the topmost layer, as being formed by the stratum corneum (SC), the epidermal layers, including the stratum granulosum (SG), the stratum spinosum (SS) and the stratum basale (SB), and the dermal layers, namely the papillary dermis (PD) and the reticular dermis (RD). The melanin-producing melanocyte cells are predominantly located in the SB layer, and the melanins can be normally found in the epidermal layers in a colloidal form or clustered in organelles known as melanosomes [5], [6]. These, in turn, can occur individually or in groups surrounded by a transparent membrane forming structures called melanosome complexes [5], [7].

Skin melanomas are often associated with a dark, nearly black color. This aspects has been mainly linked to the abundant production of dark-brown eumelamin, in comparison with red-yellow pheomelanin (Fig. 1(a)), by atypical melanocyte cells [8], [9]. However, this distinct coloration generally indicates a more advanced, deeply-invasive stage of a tumour. It has been reported that early invasive skin melanomas (EISMs) tend to exhibit a lighter, "brownish" color [10], [11].

The current understanding about the factors responsible for the chromatic attributes of EISM lesions is still far from complete, however. Besides the increased melanin production, other processes can significantly contribute to these attributes. For instance, the atypical melanocytes may be subject to an autophagy process [9], [12] in which melanosomes are sequestrated by membranous vesicles (autophagosomes) [13]. These vesicles have been observed in dermal tissues during a tumour's vertical growth phase [8], [9]. Concomitantly, angiogenesis (the process of generation of new blood vessels from pre-existing ones) may also take place to supply oxygen and nutrients to the tumour [14]–[16] by increasing the vascularity of the dermal tissues.

As the atypical melanocyte cells and new blood vessels start to occupy the PD in the early invasive stage of a melanoma lesion, tissue constituents are pushed down into the RD [17]. This process leads to an increase in the dermal blood content, which results in a higher concentration of light-absorbing hemoglobins (Fig. 1(b)). It also reduces the PD's volume fraction occupied by scattering-inducing fibrils. These alterations affect the mechanisms of light attenuation (absorption and scattering) of this tissue and, thus, the spectral responses of EISM lesions [18].

In this work, we specifically address the impact that these processes have on the EISM's chromatic attributes. Since our long-term goal is to contribute to more effective procedures for the noninvasive screening and predictive analysis of these lesions, our investigation is focused on skin melanomas classified as Clark level 2 and Breslow stage I, *i.e.*, those that have partially penetrated the PD layer [19] and have a thickness (depth) below 0.76 mm [4], respectively.

Moreover, for practical reasons, we also elected to focus on skin specimens with a relatively low level of constitutive pigmentation. It is worth noting that the lifetime risk of developing skin melanoma is larger for lightly pigmented individuals [1], [2]. This aspect, in turn, also affects the availability of supporting measured data, which often corresponds to lesions found in individuals belonging to this group. In the future, as more data becomes available, we will extend our investigation to a wide range of skin specimens (Section IV).

To overcome the practical constraints of *in vivo* experiments (*e.g.*, the modification of tissue morphological characteristics

* This work was supported by the Natural Sciences and Research Council of Canada (NSERC) under Grant 238337.

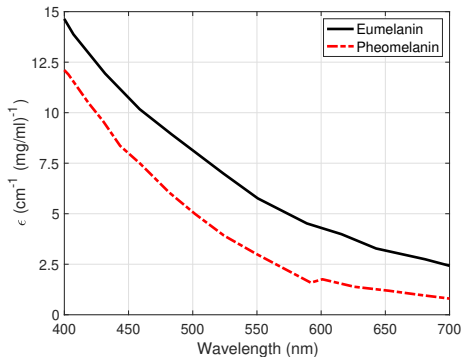

(a)

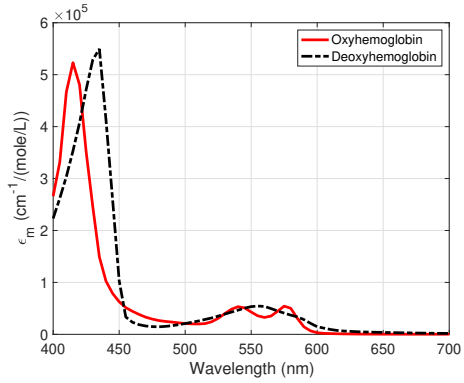

(b)

Fig. 1: Absorption spectra of two groups of visible light absorbers acting within the skin tissues. (a) Extinction coefficient (ε) curves for eumelanin and pheomelanin [20]. (b) Molar extinction coefficient (ε_m) curves for oxy- and deoxyhemoglobin [21].

on the fly), we employ an *in silico* experimental setup that builds on our previous work in this area [18]. This approach enabled us to conduct controlled experiments to systematically evaluate the sensitivity of those attributes to changes in the dermal blood contents, PD fibrils' radii and eumelanin to pheomelanin ratios (EPRs) found in atypical melanosomes. To the best of our knowledge, this is the first investigation aiming to analyze the individual and combined effects of these biophysical factors on the chromatic attributes of EISMs.

II. Materials and Methods

For context, in our previous work [18], we conducted three series of controlled *in silico* experiments. They consisted primarily in the computation of directional-hemispherical reflectance curves for normal skin and EISM specimens considering an angle of light incidence of 0°. These curves were computed using an enhanced version of the first-principles model of light and skin interactions known as HyLIoS (*H*yperspectral *L*ight *I*mpingement on *S*kin) [22]. This model employs stochastic algorithms to simulate the light attenuation processes elicited by all main absorbers and scatterers specifically acting within each of the previously mentioned cutaneous tissue layers (SC, SG, SS, SB, PD and RD). Moreover, it explicitly takes into account the intratissue distribution of melanin in colloidal and aggregated (clustered within melanosomes and melanosome complexes) forms. Accordingly, it can predictively reproduce the spectral responses of a large diversity of skin specimens with distinct levels of constitutive and facultative pigmentation [22], [23]. Its enhanced version, termed HyLIoS-MS, was specifically deployed for the simulation of skin melanoma [18]. Recall that atypical, heavily-melanized melanosomes present in melanoma lesions are found encapsulated by autophagosomes [12], [13]. These membranous vesicles are also accounted for in the melanoma simulations conducted using HyLIoS-MS.

In the first series of experiments, we computed reflectance curves for normal and EISM specimens. We then compared those curves with measured data provided by Urso *et al.* [24] in order to assess the plausibility of the specimen characterization datasets employed in the simulations. For completeness, these datasets [18] are also provided here (Tables I and II). Note that

TABLE I: Parameters kept fixed during the simulations of the spectral responses of normal and EISM specimens [18].

Description	Value
Morphological Parameters	
Ratio of Skin Surface Folds	0.1
SC Thickness (cm)	0.0008
SG Thickness (cm)	0.0033
SS Thickness (cm)	0.0033
SB Thickness (cm)	0.0033
PD Thickness (cm)	0.01
RD Thickness (cm)	0.1
Melanin Parameters	
SG Colloidal Melanin Content (%)	1.5
SS Colloidal Melanin Content (%)	1.5
SB Colloidal Melanin Content (%)	1.5
Melanosome Parameters	
Dimensions ($\mu m \times \mu m$)	0.36×0.14
Mel. Complex Diam. / Mel. Major Axis	2.0
Blood and Beta-Carotene Parameters	
Oxygenated Hemoglobin Fraction (%)	85.0
Functional Hemoglobin Concentration (g/L)	135.0
Methemoglobin Concentration (g/L)	1.5
Carboxyhemoglobin Concentration (g/L)	1.5
Bilirubin Concentration (g/L)	0.003
Beta-Carotene Concentration (g/L)	7.0E-5
SC Beta-Carotene Concentration (g/L)	2.1E-4
Epidermis Beta-Carotene Concentration (g/L)	2.1E-4
Water and Lipid Parameters	
SC Water Content (%)	35.0
Epidermis Water Content (%)	90.0
PD Water Content (%)	65.0
RD Water Content (%)	75.0
SC Lipid Content (%)	10.0
Epidermis Lipid Content (%)	1.0
PD Lipid Content (%)	5.0
RD Lipid Content (%)	5.0
Keratin, Urocanic Acid and DNA Parameters	
SC Keratin Content (%)	55.0
SC Urocanic Acid Density (mol/L)	0.01
DNA Density (g/L)	0.185
Refractive Indices	
Melanin Refractive Index	1.7
SC Refractive Index	1.55
Epidermis Refractive Index	1.4
PD Refractive Index	1.39
RD Refractive Index	1.41
Scattering Parameters	
PD Scatterers (Fibrils) Refractive Index	1.5
PD Scaterrers (Fibrils) Radius (nm)	100.0

TABLE II: Parameters employed to complement the specific characterization of the normal and EISM specimens during the simulations of their spectral responses [18].

Description	Normal	EISM
Melanosome Parameters		
SG Melanosome Content (%)	0.0	1.5
SS Melanosome Content (%)	0.0	1.5
SB Melanosome Content (%)	1.25	2.5
PD Melanosome Content (%)	0.0	8.0
Eumelanin Concentration (g/L)	32.0	41.0
Pheomelanin Concentration (g/L)	4.0	2.0
Autophagosome Parameters		
SG Encapsulated Melanosome (%)	0.0	50.0
SS Encapsulated Melanosome (%)	0.0	50.0
SB Encapsulated Melanosome (%)	0.0	50.0
PD Encapsulated Melanosome (%)	0.0	100.0
Diameter / Melanosome Major Axis	0.0	2.0
Blood Parameters		
PD Blood Content (%)	0.14	2.0
RD Blood Content (%)	0.14	2.0
Scattering Parameters		
PD Scatterers (Fibrils) Fraction (%)	22.0	14.0

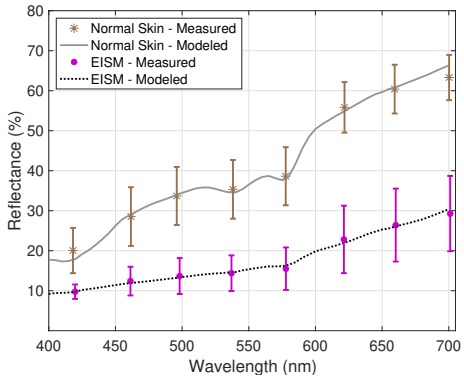

Fig. 2: Baseline reflectance datasets for a normal lightly-pigmented skin specimen and an EISM specimen. The modeled curves were computed using the HyLIoS-MS model [18]. The *in vivo* measured datasets, included for reference, were made available by Urso *et al.* [24]. The '$*$' and '$\bullet$' symbols represent measured average values, while the error bars indicate the maximum and minimum measured values obtained for 573 normal cases and 132 melanoma cases [24].

the dermal blood contents of the normal and EISM specimens were set to 0.14% and 2%, respectively, while the radius of their PD fibrils was set to 100 nm. The resulting reflectance curves for these specimens are reproduced in Fig 2. It is worth mentioning that their agreement with the measured data is markedly closer than that obtained using skin phantoms [24].

In the second series of experiments, we computed reflectance curves specifically associated with variations in dermal blood content (in both PD and RD layers), from 1 to 4% (based on the increased vascularity reported for areas adjacent to tumours [19], [27]), to assess the effects of distinct angiogenesis levels on the EISM spectral responses in the visible domain. Lastly, in the third series, we computed reflectance curves specifically associated with variations in the radius of the PD fibrils, from 100 to 60 nm (based on ranges reported for them in the literature [28], [29]), to examine how distinct magnitudes of fibril-induced scattering

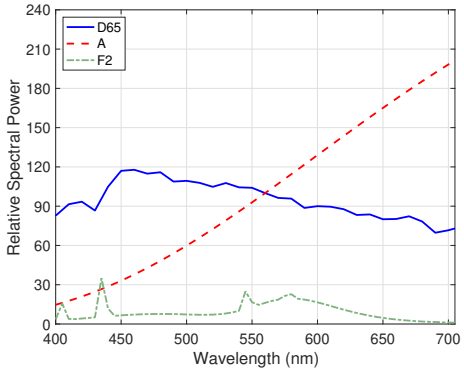

Fig. 3: Relative spectral power distributions of the selected CIE standard illuminants (D65, A and F2) [25], [26].

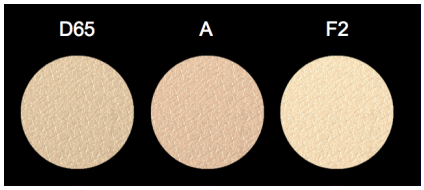

Fig. 4: Skin swatches generated using the modeled reflectance curve for a normal skin specimen provided in Fig. 2 and the selected illuminants' relative spectral power distributions presented in Fig. 3.

may affect these responses. Furthermore, to extend our scope of observations, the angiogenesis and fibril-induced scattering experiments were performed considering two different EPRs present in the atypical melanosomes encapsulated within the autophagosomes. More precisely, we have assigned to these ratios, henceforth referred to as LowEPR and HighEPR, values equal to 41:2 g/L (default value used to obtain the EISM reflectance curve depicted in Fig. 2) and 50:1 g/L (based on values reported in the literature [30], [31]), respectively. For conciseness, the reader interested in the reflectance curves obtained for the EISM specimens during the aforementioned experiments is referred to our previous publication [18].

In this work, to allow for quantitative and qualitative analyses of the impact of these pivotal parameters (dermal blood content, the PD fibril radius and the eumelanin to pheomelanin ratio) on the chromatic attributes of EISM lesions, we computed their colors through the integration of selected illuminants' relative spectral power distributions (Fig 3), the specimens' reflectance curves mentioned above and the spectral responses of the human photoreceptors [25]. To broaden the span of our chromatic comparisons, we considered three CIE (*Commission Internationale d'Eclairage*) standard illuminants, namely D65 (average daylight), A (tungsten lamp) and F2 (fluorescent lamp) [25], [26]. The integration process was then carried out using a standard CIEXYZ to sRGB color system conversion procedure [32]. Subsequently, the resulting colors were employed in the rendering of the swatches through the use of a grayscale skin texture. In Fig. 4, for illustrative purposes, we present the swatches obtained considering the normal skin specimen's reflectance curves depicted in Fig. 2.

Besides the visual inspection of the skin swatches, we also

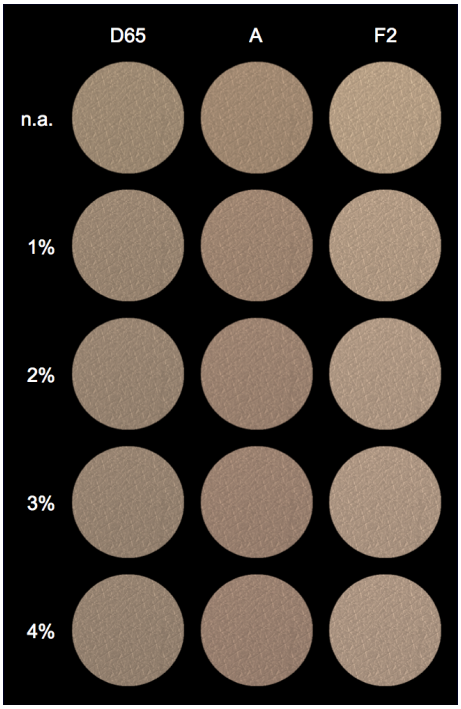

Fig. 5: Skin swatches generated for LowEPR specimens considering variations in their dermal blood contents (from 0.14% (no angiogenesis, or n.a.) to 4%) through the integration of their reflectance curves [18] with the relative spectral power distributions (Fig. 3) of the three CIE standard illuminants (D65, A and F2) considered in this investigation.

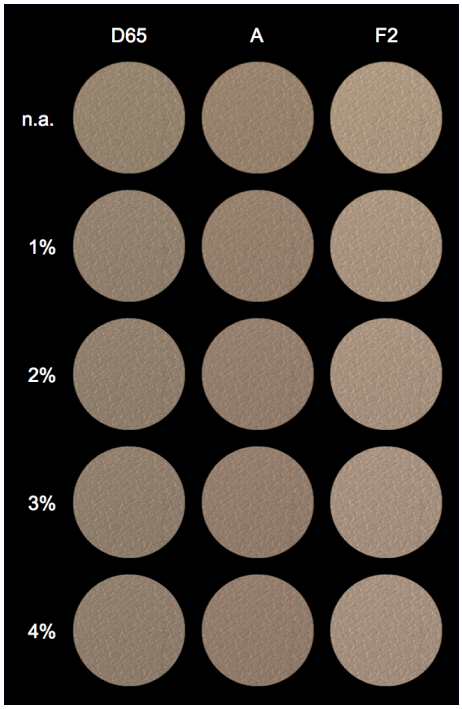

Fig. 6: Skin swatches generated for HighEPR specimens considering variations in their dermal blood contents (from 0.14% (no angiogenesis, or n.a.) to 4%) through the integration of their reflectance curves [18] with the relative spectral power distributions (Fig. 3) of the three CIE standard illuminants (D65, A and F2) considered in this investigation.

used a device-independent CIE-based metric to compare the modeled skin chromatic attributes. More precisely, we calculated the CIELAB differences between the colors (before their achromatic relative brightness modulation by the grayscale texture) associated with pairs of swatches using the following formula [33]:

$$\Delta E^*_{ab} = \sqrt{({d_L}^2 + {d_a}^2 + {d_b}^2)}, \quad (1)$$

where d_L, d_a and d_b represent the differences $L^*_1 - L^*_2$, $a^*_1 - a^*_2$ and $b^*_1 - b^*_2$, respectively, in which L^*, a^* and b^* correspond the CIELAB color space dimensions. These are calculated for the modeled chromatic attributes (colors) associated with the compared swatches (indicated by the subscripts 1 and 2). Again, we performed these calculations using standard formulas employed in colorimetry [34]. We note that it has been experimentally determined that the perceptibility threshold for these differences is ≈2.3 [33], [35], *i.e.*, chromatic variations associated with ΔE^*_{ab} values below this threshold are not considered discernible by average human observers.

III. Results and Discussion

In Fig. 5, we present the swatches generated for the specimens with distinct dermal blood contents and LowEPR. It can be observed that they become slightly darker as we considered larger blood contents. This aspect aligns with the increase in light absorption prompted by a higher concentration of hemoglobins [21]. This trend, in turn, leads to higher CIELAB chromatic differences as it can be verified by inspecting the ΔE^*_{ab} values provided in Table III.

TABLE III: ΔE^*_{ab} values calculated for the swatches of LowEPR (Fig. 5) and HighEPR (Fig. 6) specimens with respect to the swatches of specimens with a dermal blood content equal to 0.14% (no angiogenesis).

Dermal Blood Content	LowEPR Specimens			HighEPR Specimens		
	Illuminants			Illuminants		
	D65	A	F2	D65	A	F2
1%	1.55	2.27	2.29	0.92	1.28	1.51
2%	**2.86**	**3.49**	**3.54**	2.22	**2.30**	**2.78**
3%	**3.23**	**3.71**	**4.41**	**2 .50**	**2.63**	**3.03**
4%	**3.88**	**4.48**	**5.04**	**2.62**	**3.03**	**3.82**

Values $\geq$ 2.3 (perceptibility threshold) are presented in boldface.

In Fig. 6, we present the swatches generated for the specimens with distinct dermal blood contents and HighEPR. Similarly, it can be observed that they become slightly darker as we considered larger blood contents. Also, they appear darker than those depicted in Fig. 5, which conforms with the increased presence of eumelanin, a stronger absorber than pheomelanin in the visible spectral domain (Fig. 1). However, the transition from the lightest hue to a darker hue becomes perceptible ($\Delta E^*_{ab} \geq 2.3$) under all three illuminants for the specimens associated with a 3% dermal blood content, while for the LowEPR specimens this was true for a 2% dermal blood content. These observations are also consistent the ΔE^*_{ab}

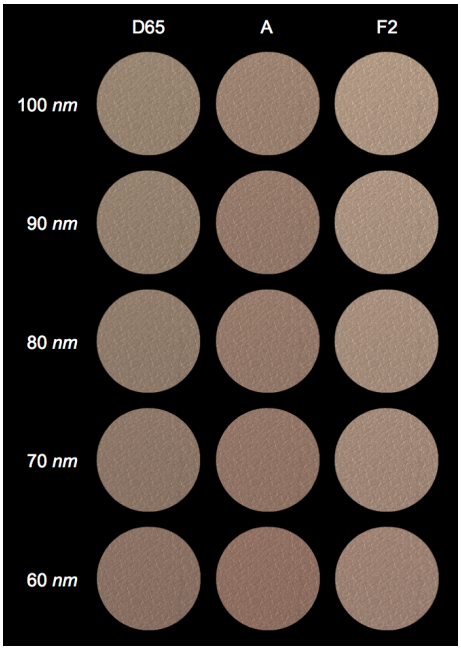

Fig. 7: Skin swatches generated for LowEPR specimens considering variations in their papillary dermis fibril radius (from 100 to 60 nm) through the integration of their reflectance curves [18] with the relative spectral power distributions (Fig. 3) of the three CIE standard illuminants (D65, A and F2) considered in this investigation.

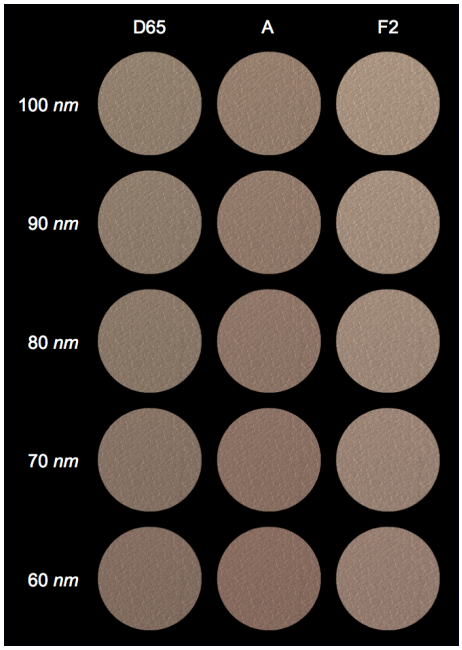

Fig. 8: Skin swatches generated for HighEPR specimens considering variations in their papillary dermis fibril radius (from 100 to 60 nm) through the integration of their reflectance curves [18] with the relative spectral power distributions (Fig. 3) of the three CIE standard illuminants (D65, A and F2) considered in this investigation.

values provided in Table III.

In Fig. 7, we present the swatches generated for the specimens with distinct PD fibril radius and LowEPR. It can be observed that the swatches associated with lower values of this parameter were noticeably darker. This can be explained by the fact that a reduction in the PD fibril radius leads to a decrease in fibril-induced (Rayleigh-type) scattering [36]–[38]. The same trend can be observed for the swatches generated for specimens with distinct PD fibril radius and HighEPR which are presented in Fig. 8. They appear, however, slightly darker due the increased presence of eumelanin.

It can also be observed in Figs. 7 and 8 that the transitions from the lightest hue (specimens with a 100 nm PD fibril radius) to the darkest hue (specimens with a 60 nm PD fibril radius) were more noticeable than the lightest to the darkest hue transitions associated with the variations in the dermal blood content (from 0.14% to 4%, respectively) depicted in Figs. 5 and 6. This can be further verified by comparing the ΔE^*_{ab} values presented in Tables III and IV. This aspect highlights the complexity of the processes responsible for the chromatic attributes of EISMs, whose appearance may be also significantly affected by other factors besides the abnormal presence of light-absorbing pigments [8], [39].

Although visual differences between EISMs with significantly distinct characterizations (*e.g.*, the lightest and darkest hue cases mentioned above) can be readily noticeable, visual differences elicited by incremental variations is these characterizations may not be easily perceived. For instance, variations in dermal blood content on the order of 1% resulted in CIELAB chromatic differences below the perceptibility threshold ($\Delta E^*_{ab} < 2.3$) as indicated in Table V. Similarly, variations in the PD fibril radius on the order of 10 nm resulted in differences below this threshold in all but one case as shown in Table VI. Hence, relatively small incremental variations in the biophysical characteristics of these lesions cannot be reliably detected through the visual examination of changes in the chromatic attributes of EISMs.

TABLE IV: ΔE^*_{ab} values calculated for the swatches of the LowEPR (Fig. 7) and HighEPR (Fig. 8) specimens with respect to the swatches of specimens with a PD fibril radius equal to 100 nm.

	LowEPR Specimens			HighEPR Specimens		
	Illuminants			Illuminants		
PD Fibril Radius	D65	A	F2	D65	A	F2
90 nm	1.33	1.52	1.58	1.27	1.18	1.59
80 nm	**3.20**	**3.04**	**3.60**	**2.91**	**3.20**	**3.63**
70 nm	**4.80**	**5.02**	**5.96**	**4.84**	**4.61**	**5.58**
60 nm	**6.85**	**6.99**	**7.62**	**6.91**	**6.54**	**7.43**

Values ≥ 2.3 (perceptibility threshold) are presented in boldface.

We remark that the main factors generally associated with the distinct coloration of skin melanomas are the abnormal presence of melanin and the ratio of eumelanin to pheomelanin [8], [9]. Although our *in silico* findings are consistent with these aspects, they also suggest that the increased presence of hemoglobins resulting from angiogenesis and the specific morphological characteristics of the affected skin site, such as the PD fibril radius, should not be overlooked, particularly with respect to EISMs. They also highlight the fact that, although these lesions have chromatic attributes markedly distinct from the surrounding normal cutaneous tissues (*e.g.*, Fig. 4), their

coloration is also far from the strong dark hues of deeply invasive melanomas [8].

More common skin spots with increased pigmentation, such as freckles, often exhibit a "brownish" coloration. This indicates that coloration alone cannot be used as a reliable EISM lesion indicator. However, combined with other criteria, such as the lesions' asymmetry and atypical border [3], the "brownish" coloration may provide a visible warning about an EISM and its possible progression to a more serious, metastatic stage. Also, as the brown hues become progressively darker, they may provided additional clues about its evolution and the underlying processes taking place such as autophagy [9], [13] and angiogenesis [17], [18].

Our *in silico* experiments also enabled us to assess the effects that different illuminants may have on the perceived appearance of the EISM specimens. Although all three selected illuminants led to a "brownish" coloration, some appearance differences, similar to those observed in the swatches generated for the normal skin specimens (Fig. 4) were also noticeable in the swatches generated for the EISM specimens (Figs. 5 to 8). For instance, the swatches obtained using illuminant A displayed a red tinge associated with the stronger red component of this illuminant's relative spectral power distribution (Fig. 3). Also, even though the same light intensity was employed in the generation of all swatches, those obtained using illuminants D65 and A displayed a seemingly darker appearance than the swatches obtained using illuminant F2. This observation illustrates how color perception issues associated with the human visual system may affect the interpretation of lesion appearance traits, particularly under distinct illumination conditions. Thus, they may inadvertently bias screening protocols and workflows employed in clinical practice, which, as mentioned earlier, have as one of their key steps the visual inspection of lesion coloration [3], [4].

In short, the visual signs provided by changes in the appearance traits of melanomas, notably their coloration, are an integral part of the screening protocols and workflows used in the noninvasive assessment of these lesions at the point of care. However, as suggested by our findings, their correct interpretation may be affected not only by the aggregated effects of different biophysical factors, but also by the limitations of the human visual system. Moreover, color perception phenomena, such as metamerism (in which the perceived colors of two specimens match under a specified illuminant and a specified observer even though their reflectances differ in the visible domain [34], [40]), need to be considered as well. Hence, whenever possible, the noninvasive assessment and predictive analysis of these lesions should also include the optical inspection of their reflectance responses [18]. It is important to note that the measurement of these responses may be subject to technical issues (*e.g.*, influence of probe pressure on the reading's accuracy [41]) that also need to be addressed.

IV. Conclusion and Future Work

We have examined how different biophysical factors can contribute to the coloration of EISM lesions. Although this appearance trait may not be sufficient for their effective screening, it can provide useful information for their timely detection and correct staging. These aspects, in turn, can increase the probability of a positive prognosis with respect to their treatment.

TABLE V: ΔE^*_{ab} values calculated for pairs of swatches of LowEPR specimens (Fig. 5) and for pairs of swatches of HighEPR specimens (Fig. 6), with the successive pairs associated with increasing dermal blood contents.

Dermal Blood Content	LowEPR Specimens			HighEPR Specimens		
	Illuminants			Illuminants		
	D65	A	F2	D65	A	F2
0.14% - 1%	1.55	2.27	2.29	0.92	1.28	1.51
1% - 2%	1.32	1.27	1.27	1.33	1.15	1.28
2% - 3%	0.64	0.39	0.90	0.39	0.35	0.38
3% - 4%	0.60	0.94	0.64	0.45	0.45	0.39

TABLE VI: ΔE^*_{ab} values calculated for pairs of swatches of LowEPR specimens (Fig. 7) and for pairs of swatches of specimens HighEPR (Fig. 8), with the successive pairs associated with decreasing PD fibril radii.

PD Fibril Radii	LowEPR Specimens			HighEPR Specimens		
	Illuminants			Illuminants		
	D65	A	F2	D65	A	F2
100 nm - 90 nm	1.33	1.52	1.58	1.27	1.18	1.59
90 nm - 80 nm	2.20	1.53	2.05	1.64	2.23	2.07
80 nm - 70 nm	1.61	2.07	**2.41**	2.06	1.56	1.98
70 nm - 60 nm	2.23	2.08	2.18	2.24	2.07	1.99

Values $\geq$ 2.3 (perceptibility threshold) are presented in boldface.

The interconnected biophysical phenomena responsible for the chromatic attributes of skin melanomas are complex and still not completely understood. Before reaching a deeply invasive stage, often characterized by a strong dark coloration, these lesions may undergo morphological and physiological alterations that affect their chromatic attributes. The correct interpretation of these attributes relies on the understanding about their eliciting biophysical factors as well as their observation conditions.

Our *in silico* findings show that variations in these attributes, albeit markedly affected by the abnormal production of melanin, can be also significantly modulated by the increased presence of other pigments, notably the hemoglobins, and the intrinsic characteristics of the affected dermal tissues such as the radius of the PD fibrils. Moreover, they also show that colorimetric aspects, such as the relative lightness and hues depicted by the lesions, can be noticeably influenced by the illuminants' radiometric properties, in particular their relative spectral power distributions.

As future work, we plan to examine the effects of variations in other biophysical parameters such as blood oxygenation, as well as extend our investigation to other tumour phase transitions and different skin phototypes. The advance of the current knowledge about the spectral and colorimetric responses of skin melanomas cannot rely solely on computational studies, however. More high-quality measured datasets are required to

enhance the fidelity of modeled predictions, which, in turn, can be synergistically employed to expand the scientific reach of experimental initiatives in this area.

REFERENCES

[1] D. Schadendorf, A.C.J. van Akkooi, C. Berking, K.G. Griewank, R. Gutzmer, A. Hauschild, A. Stang, A. Roesch, and S. Ugurel, "Melanoma," *Lancet*, vol. 392, pp. 971–984, 2018.

[2] R.L. Siegel, T.B. Kratzer, A.N. Giaquinto, H. Sung, and A. Jemal, "Cancer statistics, 2025," *CA Cancer J. Clin.*, vol. 75, pp. 10–45, 2025.

[3] P. Carli, V. de Giorgi, D. Palli, and V. Giannotti, "Preoperative assessment of melanoma thickness by ABCD score of dermatoscopy," *J. Am. Acad. Dermatol.*, vol. 43, no. 3, pp. 459–466, 2000.

[4] L.E. Davis, S.C. Shalin, and A.J. Tackett, "Current state of melanoma diagnosis and treatment," *Cancer Biol. Ther.*, vol. 20, no. 11, pp. 1366–1379, 2019.

[5] R.L. Olson, J Gaylor, and M.A. Everett, "Skin color, melanin, and erythema," *Arch. Dermatol.*, vol. 108, no. 4, pp. 541–544, 1973.

[6] M.A. Pathak, "Functions of melanin and protection by melanin," in *Melanin: Its Role in Human Photoprotection*, M.R. Chedekel L. Zeise and T.B. Fitzpatrick, Eds., Overland Park, Kansas, USA, 1995, pp. 125–134, Valdenmar Publishing Co.

[7] G. Szabo, A. Gerald, M. Pathak, and T.B. Fitzpatrick, "Racial differences in the fate of melanosomes in human epidermis," *Nature*, vol. 222, no. 5198, pp. 1081–1082, 1969.

[8] R. Lazova and J.M. Pawelek, "Why do melanomas get so dark?," *Exp. Biol.*, vol. 18, pp. 934–938, 2009.

[9] R. Lazova, V. Klump, and J.M. Pawelek, "Autophagy in cutaneous malignant melanoma," *J. Cutan. Pathol.*, vol. 37, pp. 256–268, 2010.

[10] I. Stanganelli, G. Argenziano, F. Sera, A. Blum, F. Ozdemir, I.K. Karaarslan, D. Piccolo, K. Peris, H. Kirchesch, R. Bono, M.A. Pizzichetta, S. Gasparini, R.P. Braun, O. Correira, L. Thomas, P. Zaballos, S. Puig, J. Malvehy, M. Scalvenzi, H. Rabinovitz, A. Bergamo, G. Pellacani, C. Longo, M. Pavlovic, C. Rosendahl, R. Hofmann-Wellenhof, H. Cabo, A.A. Marghoob, D. Langford, S. Astorino, A.M. Manganoni, J.Y. Gourhant, J. Keir, J.M. Grichnik, G. Fumo, H. Dong, A.M.S. Rachou, G. Ferrara, and I. Zalaudek, "Dermoscopy of scalp tumours: A multi-centre study conducted by the Int. Dermoscopy Soc.," *J. Eur. Acad. Dermatol. Venerol.*, vol. 26, no. 8, pp. 953–963, 2011.

[11] S. Polesie, E. Jergeus, M. Gillstedt, H. Ceder, J.D. Gyllencreutz, J. Fougelberg, E.J. Backman, J. Pakka, O. Zaar, and J. Paoli, "Can dermoscopy be used to predict if a melanoma is *in situ* or invasive?," *Dermatol. Pract. Concept.*, vol. 11, no. 3, pp. e2021079:1–6, 2021.

[12] D. Murase, A. Hachiya, K. Takano, R. Hicks, M.O. Visscher, T. Kitahara, T. Hase, Y. Takema, and T. Yoshimori, "Autophagy has a significant role in determining skin color by regulating melanosome degradation in keratinocytes," *J. Invest. Dermatol.*, vol. 133, pp. 2416–2424, 2013.

[13] M. Jin and D.J. Klionsky, "Regulation of autophagy: Modulation of the size and number of autophagosomes," *FEBS Lett.*, vol. 588, no. 15, pp. 2457–2463, 2014.

[14] J. Marcoval, A. Moreno, J. Graells, A. Vidal, J.M. Escribà, M. Garcia-Ramirez, and A. Fabra, "Angiogenesis and malignant melanoma. Angiogenesis is related to the development of vertical (tomorigenic) growth phase," *J. Cutan. Pathol.*, vol. 24, pp. 212–218, 1997.

[15] M. Streit and M. Detmar, "Angiogenesis, lymphangiogenesis, and melanoma metastasis," *Oncogene*, vol. 22, pp. 3172–3179, 2003.

[16] D.A. Hormuth II, C.M. Phillips, C. Wu, E.A.B.F. Lima, G. Lorenzo, P.K. Jha, A.M. Jarret, J.T. Oden, and T.E. Yankeelov, "Biologically-based mathematical modeling of tumor vasculature and angiogenesis via time-resolved imaging data," *Cancers*, vol. 13, pp. 3008:1–28, 2021.

[17] H. Kamino, S. Tam, D. Roses, and S. Toussaint, "Elastic fiber pattern in regressing melanoma: A histochemical and immunohistochemical study," *J. Cutan. Pathol.*, vol. 37, pp. 723–729, 2010.

[18] G.V.G. Baranoski and P.M. Varsa, "Angiogenesis-elicited spectral responses of early invasive skin melanoma: Implications for the evaluation of lesion progression," *J. Biophotonics*, vol. 17, pp. 202400208:1–13, 2024.

[19] L.C.L.T. van Kempen, J. Rijntjes, I. Mamor-Cornelissen, S. Vincent-Naulleau, M.P. Gerritsen, D.J. Ruiter, M.C.R.F. van Dijk, C. Geffrotin, and G.N.P. van Muijen, "Type I collagen expression contributes to angiogenesis and the development of deeply invasive cutaneous melanoma," *Int. J. Cancer*, vol. 122, pp. 1019–1029, 2008.

[20] S.L. Jacques, "Optical absorption of melanin," Tech. Rep., Oregon Medical Laser Center, OR, USA, 2001.

[21] S.A. Prahl, "Optical absorption of hemoglobin," Tech. Rep., Oregon Medical Laser Center, OR, USA, 1999.

[22] T.F. Chen, G.V.G. Baranoski, B. Kimmel, and E. Miranda, "Hyperspectral modeling of skin appearance," *ACM Trans. Graph.*, vol. 34, no. 3, pp. 31:1–14, 2015, Supplemental video: https://www.youtube.com/watch?v=hKvIWS5H94s.

[23] T.F. Chen and G.V.G. Baranoski, "A physiologically-based framework for the simulation of skin tanning dynamics," in *Proc. of SPIE, Vol. 10877, Dynamics and Fluctuations in Biomedical Photonics XVI: Tissue and Cell Dynamics, SPIE Photonics West - BiOS*, M.J. Leahy V.V. Tuchin and R.W. Wang, Eds., San Francisco, CA, USA, March 2019, pp. 108770H–1–20, Supplemental video: https://www.youtube.com/watch?v=I1quYM34wWw.

[24] P. Urso, M. Lualdi, A. Colombo, M. Carrara, S. Tomatis, and R. Marchesini, "Skin and cutaneous melanocytic lesion simulation in biomedical optics with multilayered phantons," *Phys. Med. Biol.*, vol. 52, pp. N229–N239, 2007.

[25] R.W.G. Hunt, *Measuring Colour*, Ellis Horwood Limited, Chichester, England, 2nd edition, 1991.

[26] N. Ohta and A.R. Robertson, *Colorimetry Fundamentals and Applications*, John Wiley & Sons, New York, NY, USA, 1982.

[27] J. Welzel, S. Schuh, N. de Carvalho, L. Themstrup, M. Ulrich, G.B.E. Jemec, and J. Holmes G. Pellacani, "Dynamic optical coherence tomography shows characteristic alterations of blood vessels in malignant melanoma," *JEADV*, vol. 35, pp. 1087–1093, 2021.

[28] R.L. Hayes and G.P. Rofnan, "The ultrastructure of skin in progressive sclerosis (scleroderma) I. dermal collagen fibers," *Am. J. Pathology*, vol. 63, no. 3, pp. 433–440, 1971.

[29] H. Arao, M. Obata, T. Shimada, and S. Hagisawa, "Morphological characteristics of the dermal papillae in the development of pressure sores," *J. Tissues Viability*, vol. 8, no. 3, pp. 17–23, 1998.

[30] A. J. Thody, E. M. Higgins, K. Wakamatsu, S. Ito, S. A Burchill, and J. M. Marks, "Pheomelanin as well as eumelanin is present in human epidermis," *J. Invest. Dermatol.*, vol. 97, no. 2, pp. 340–344, 1991.

[31] A. Hennessy, C. Oh, B. Diffey, K. Wakamatsu, S. Ito, and J. Rees, "Eumelanin and pheomelanin concentrations in human epidermis before and after UVB irradiation," *Pigment Cell Res.*, vol. 18, pp. 220–223, 2005.

[32] G.V.G. Baranoski and A. Krishnaswamy, *Light & Skin Interactions: Simulations for Computer Graphics Applications*, Morgan Kaufmann/Elsevier, Burlington, MA, USA, 2010.

[33] M. Stokes, M.D. Fairchild, and R.S. Berns, "Precision requirements for digital color reproduction," *ACM Trans. Graph.*, vol. 11, no. 4, pp. 406–422, 1992.

[34] D.H. Brainard, "Color appearance and color difference specification," *The Science of Color*, vol. 2, pp. 191–216, 2003.

[35] M. Mahy, L. Van Eycken, and A. Oosterlinck, "Evaluation of uniform color spaces developed after the adoption of CIELAB and CIELUV," *Color Res. Appl.*, vol. 19, no. 2, pp. 105–121, 1994.

[36] S.L. Jacques, "Origins of tissue optical properties in the UVA, visible, and NIR regions," *OSA Proc. Adv. Opt. Imaging and Photon Migration*, vol. 2, pp. 364–369, 1996.

[37] S.R. van Leeuwen and G.V.G. Baranoski, "Elucidating the contribution of Rayleigh scattering to the bluish appearance of veins," *J. Biomed. Opt.*, vol. 23, no. 2, pp. 025001–1–17, 2018.

[38] S.R. van Leeuwen and G.V.G. Baranoski, "Can reduced scattering coefficients obtained using inversion procedures lead to unsound inferences about the optical factors contributing to the appearance of blood vessels embedded in the skin?," Tech. Rep. CS-2019-01, School of Computer Science, University of Waterloo, Ontario, Canada, 2019.

[39] R. Marchesini, A. Bono, and M. Carrara, "*In vivo* characterization of melanin in melanocytic lesions: Spectroscopic study on 1671 pigmented skin lesions," *J. Biomed. Opt.*, vol. 14, no. 1, pp. 014027–1–18, 2009.

[40] ASTM, "Standard terminology of appearance," Tech. Rep. E284-17, ASTM (American Society for Testing and Materials), International, West Conshohocken, PA, USA, 2017.

[41] J.A.D. Atencio, E.E.O. Guillén, S.V. Montiel, M.C. Rodríguez, J.C. Ramos, J.L. Gutiérrez, and F. Martínez, "Influence of probe pressure on human skin diffuse reflectance spectroscopy measurements," *Optical Memory and Neural Networks*, vol. 18, no. 1, pp. 6–14, 2009.